Study of Thermal Fatigue of H13 Die Steel with Various Surface Treatments

*V.V.Ivanov, **I.R.Paine and ***P.J.Revnyuk

**The University of Auckland, New Zealand.*
***Glucina Smelters Limited, New Zealand.*
****UkrNDITSM, Ukraine*

(Received November 26, 2001)

ABSTRACT

Surfaces of die casting dies are subjected to very severe conditions of cyclical thermal and mechanical load, and chemical and mechanical wear. Dies mostly fail due to a combination of heat checking, erosion, corrosion and soldering.

It is conceivable that appropriate surface treatments and coatings have a favourable influence on the temperature dependant performance of the surface of the die.

The objective of this study was to examine various surface treatments and coatings, including shot peening, nitriding, nitrocarburizing, laser hardening and remelting, electro-spark alloying (deposition) and plasma spraying under thermal fatigue conditions.

Thermal cycling tests were conducted by alternate dipping of treated samples in an LM24 melt and in water. Results and their analyses are presented in this paper. The best thermal fatigue resistance was shown by the specimen which had a double treatment of laser hardening plus electro-spark deposition.

INTRODUCTION

In service, die casting dies are subjected alternately to heating and cooling. When hot metal strikes the surface of the die, the die expands and then contracts during cooling, as the heat in the casting is conducted into the steel below the surface of the die. This gives rise to severe strains in the surface layer of the material, gradually leading to thermal fatigue cracks. Cracking occurs when the cavity surface is under tensile stress in the shot cycle, i.e. during the cooling part at the low temperature end. High peak temperatures and rapid cooling increase this risk. The result can be a pattern of surface cracks and this phenomenon is known as "heat checking". This process is one of the main causes of die failures.

Heat checking is a fatigue phenomenon and follows the laws of fatigue, i.e. a starting (initiation) period and growing (propagation) period. Thermal fatigue nucleation and growth can be described by the Coffin-Manson and the Paris (Solomon) equations, respectively /1/. These models indicate that the number of cycles to nucleate cracks, as well as their growth, vary exponentially with the plastic strain amplitude.

Thermal fatigue occurs at the high stress end of the *S-N* curves, which corresponds to a low cycle fatigue /2/. During heating, a die surface expands and, due to the interaction with the cold die core, it is subjected to plastic compression. During cooling, the elongated surface will contract, which generates tensile stress on it. The total deformation is given by:

$$\Delta\varepsilon = \Delta\varepsilon_e + \Delta\varepsilon_p \qquad (1)$$

However, under a low cycle regime, plastic strain is quantitatively more relevant than elastic strain. The

"strain amplitude – number of cycles" curve shows the Coffin-Manson relationship /3/:

$$\Delta\varepsilon_p = \varepsilon'_f N_f^c \quad (2)$$

where N_f is a life, measured in number of cycles to failure, ε'_f is a fatigue ductility coefficient and c is the fatigue ductility exponent.

Malm and Norstrom analysed the relationship between plastic strain amplitude during thermal fatigue, $\Delta\varepsilon_p$, and mechanical properties of materials /4/. They found:

$$\Delta\varepsilon_p = \alpha(T_2 - T_1) - (1 - \eta_2)\sigma_2 / E_2 - (1 - \eta_1)\sigma_1 / E_1 \quad (3)$$

where α is the thermal expansion coefficient, η - Poisson's ratio, σ - yield strength, and E - modulus of elasticity. The indices 1 and 2 correspond to T_1 and T_2 temperatures. This model indicates that high thermal fatigue resistant materials should have a low thermal expansion coefficient, a low Poisson coefficient and a high yield strength to modulus of elasticity ratio. Oxidation resistance and residual compressive stress also contribute to raising the thermal fatigue resistance /2/.

Hard coatings are usually characterised by hot yield strength (hot hardness) and tempering resistance significantly greater than that of tool steels. On the other hand, strain fracture of hard coatings, even though unknown, is expected to be much lower than that of tool steels. However, the fact that hard coatings come with compressive stresses may compensate the latter drawback. Taking all these facts into consideration it can be expected that the coated samples will have better checking resistance.

After initiation the fatigue crack grows at a rate described by Paris equation:

$$dc/dN = C(\Delta K)^m \quad (4)$$

where ΔK, the opening mode stress intensity factor, is above a threshold value, dc/dN is the crack size increment per cycle, C and m are constants. The stress intensity factor ΔK increases with stress amplitude, which, in turn, increases with ΔT.

During heating, the coatings, which have a lower coefficient of thermal expansion than tool steels, will expand several times less than the substrate. The coated substrate will therefore deform less than the uncoated one, which will result in a lower stress intensity factor and, consequently, in a lower crack growth rate. Furthermore, the residual compressive stresses in the coatings and nitrided layer reduce the stress intensity factor at the nucleated crack tip, reducing the crack growth rate in the substrate.

It is also important to control the defect density in the coatings. A solution to this might be the use of multilayered coatings with different thermal and mechanical properties. Defects in one layer would be nullified by the subsequent layer, resulting in reduction of the overall defect density /5/.

Compressive residual stresses produced by shot peening or, in other words, by surface plastic deformation, are usually regarded as the major factor in increasing fatigue strength /6/. The normal surface tensile stresses that are inherent in a die after finish machining, grinding and heat treating are converted into compressive stresses. The maximum compressive stresses profile has a subsurface penetration of 100-200 μm and this inhibits the propagation of already initiated cracks.

PROCEDURE

A combined Erosion/Corrosion/Thermal Cycling Test Apparatus was designed and built at Glucina Smelters Limited to simulate the aluminium die casting conditions and to be able to test multiple specimens at the same time (Figure 1). The testing apparatus consists of:

1) electrical furnace with two thermocouples, to maintain the molten aluminium temperature within ± 5°C;
2) bath with water;
3) samples holder with an electric drill, which is able to rotate specimens in molten aluminium at various speeds;
4) pneumatic system, which provides alternating exposure of testing samples in molten aluminium and water;
5) automatic controlling system, which allows regulating a holding time, movement speed, and displays the number of cycles.

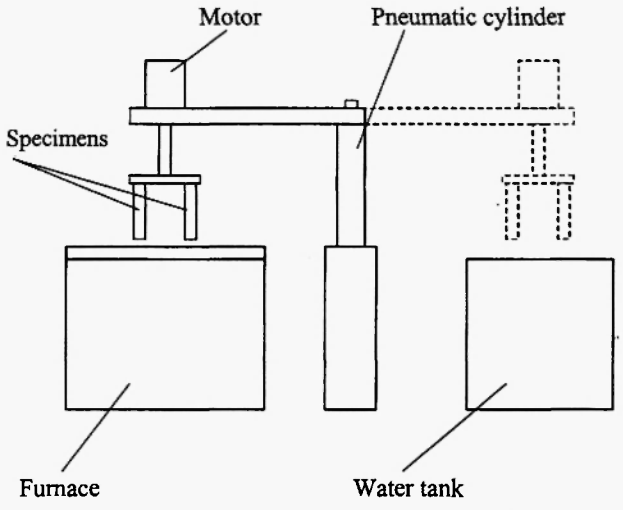

Fig. 1: Schematic diagram of the combined thermal fatigue/erosion/corrosion test rig.

The melt was aluminium die casting alloy LM24 (BS 1490), which was maintained at a temperature of 700°C. The water bath consisted of tap water and a commercial die lubricant RDL-2588. During the test, water was replenished and also cooled down by compressed air to maintain a temperature of 90 ± 5°C.

Six samples were tested at one time, giving a good comparison under identical testing conditions. The base metal was H13 tool steel with the following composition (%): C 0.4, Cr 5.25, Mo 1.5, V 1.0, Si 1.0, Mn 0.35. The specimens were machined and ground by a commercial die manufacturer to a final size of 13 mm-square and 150 mm-length with a 15 mm-depth threaded hole from one side. The grinding pattern was normal to the length of a specimen. Next, heat treatment, surface treatment and coating were applied to the samples. The selected treatments are shown in Table 1.

All specimens were treated with anti-soldering paste (commonly called *Antilova*) to prevent molten aluminium sticking to the surface. The bare H specimens were more inclined to have the soldering problem.

The specimens were dipped into the molten aluminium for 7 sec., lifted out over the water bath and immersed into the water for 10 sec. After that, samples were held above the molten aluminium for 4 sec. This completed one cycle. During one day 1000 cycles were completed. After every 1000 cycles, the specimens were removed from the holding plate to get rid of excessive oxide and lubricant residue build-up. The samples were cleaned by rubbing them against 500-grit silicon carbide paper on a glass plate. A 5-mm piece was cut off each

Table 1
Selected treatments and coatings

Code	Heat Treatment	Surface Treatment and Coating
H4	Austenitising at 1040°C, 40 min.; double tempering at 540°C, and 595°C.	
N1	- " -	Conventional Nitriding, 510°C.
N2	- " -	Ferritic Nitro-Carburising (FNC), 580°C.
N3	- " -	Controlled Gas Nitriding (Nitreg-Process).
S	- " -	Shot Peening: diameter of shots - 1.1 mm; pressure – 0.23 MPa; coverage – 200%; intensity (arc height on A-strip) – 0.25 mm.
L1	- " -	TK6 (WC/Co); by Electro Spark Deposition (ESD).
L2	- " -	Laser Hardening (KVANT-100).
L3	- " -	Laser Hardening + TK6 (WC,Co) by ESD.
P1	- " -	Ni/Al + Y-stabilised Zr; by Plasma-Sprayed Coating (PSC).
P2	- " -	Co-based Superalloy by PSC.

specimen for examination after 1500, 5000, 10000, 15000, 20000 and 25000 cycles.

Macro- and Microstructure

After 25000 cycles, the oxide layer was removed completely by gradual grinding from 220-grit to 1200-grit paper for crack evaluation. Corners of each specimen were examined under an optical microscope at a magnification of 25× and 100×. The examined area was 10 mm long and was located at 30 mm from the bottom end of the specimen to avoid any end effects. The thermal fatigue resistance was evaluated based on crack parameters, defined as:

- l_{max}, the maximum crack length;
- Σl_{max}, the accumulated crack length;
- l_{av}, the average crack length;
- n, the number of cracks per unit of length.

Transverse surfaces of each specimen were prepared for metallographic examination using the standard polishing technique. Samples were etched in 2.5% Nital for 20-60 sec. so that the general microstructure could be observed. The specimens were examined in the etched condition at magnifications of 100×, 200× and 500×.

Hardness and Microhardness

Hardness of the surface layer and subsurface material was measured using a Wilson/Rockwell Hardness Tester, Series 500. To determine the hardness of the microstructural constituents a M-400 Microhardness Tester was used.

Phase Analysis

X-ray diffraction was used to establish the phases by identifying the peaks present in the Joint Committee for Powder Diffraction Standards (JCPDS) data. The XRD patterns were obtained using a Philips Powder Diffractometer PW 1729 operating in Bregg-Brentanno geometry with CoK_{α} radiation (1.79021). The data was collected in the range of 15 - 140° by steps of 0.1° with the goniometer speed of 0.1°/sec, using the Visual XRD Software. Data was displayed on the screen as it was collected. The collected data was analysed using the Traces V.4.0 Software.

Scanning Electron Microscopy (SEM)

The morphology of specimen surfaces was studied by SEM. The SEM patterns were obtained using the Philips SEM 505 at the accelerating voltage of 20 kV.

Energy Dispersive X-ray (EDX) Analysis

The content and distribution of the alloying elements in the various layers and phases was investigated using the EDX. The EDX patterns were obtained using the EDX PGT System at the accelerating voltage of 20 kV.

RESULTS AND DISCUSSION

Surface defects, which were observed on the tested specimens after 25000 cycles are listed in Table 2. The coating of the plasma sprayed specimen P1 has broken off the corners up to 3 mm and was withdrawn from the testing program after 10000 cycles.

H-type Specimens

The transverse crack pattern of the H4 specimen after 25000 cycles is shown in Figure 2. The cracks have a pronounced tapering structure, which means that they were opening up. The surface hardness values had dropped from (475 – 525) H_v at the beginning to (290 – 305) H_v after the first 1500 cycles and maintained the same level up to the end of the test.

There is a feature, which is common only for H-type specimens – it is the presence of pit-like defects (Figures 3 and 4). They are filled in with two different substances of grey and white appearance in the picture. The EDX analyses have shown the presence of Fe, Cr, Si, V, and Mn in the grey one. The XRD results were not very convincing showing complex oxides as well as intermetallic compounds, but taking into consideration the microhardness values of (550 - 750) H_v, it is quite reasonable to conclude that the grey substance mostly consists of the complex spinel-type oxides. The EDX analyses of the white substance have shown the

Table 2
Surface defects of the tested specimens after 25000 cycles.

Code	Transverse Cracks				Longitudinal Cracks				Pit-like Defects
	l_{max}, μm	Σl, μm	l_a, μm	n, cr./mm	d_{max}, μm	Σd, μm	d_a, μm	n, cr./mm	
H4	370	5330	232	2.3	-	-	-	-	present
N1	600	6640	316	2.1	100	1640	63	0.50	-
N2	520	4270	251	1.7	70	300	50	0.12	-
N3	480	6310	287	2.2	30	390	33	0.23	-
S	270	3950	208	1.9	-	-	-	-	-
L1	120	1150	96	1.2	-	-	-	-	-
L2	180	2880	131	2.2	-	-	-	-	-
L3	80	700	70	1.0	-	-	-	-	-
P2	240	2800	140	2.0	-	-	-	-	-

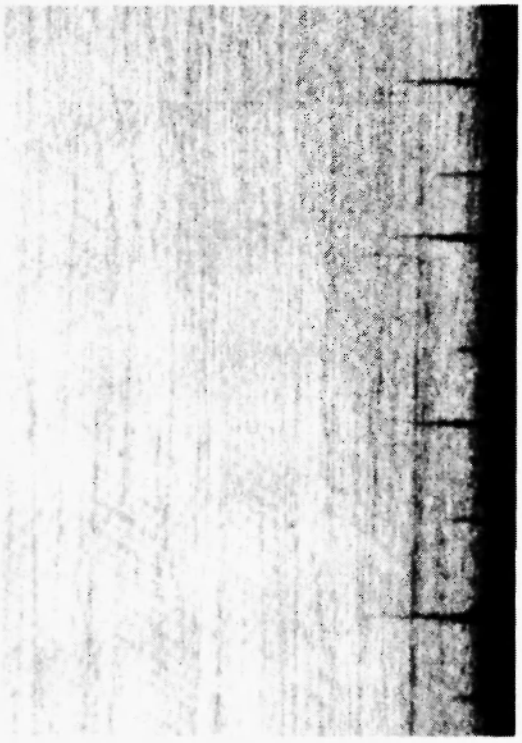

Fig. 2: Transverse crack pattern of the H4 specimen, 25000 cycles, 25×.

presence of Al, Fe, Si, Cr and V, and taking into account the microhardness values of (950 – 1050) H_v, it could be intermetallic compounds /7/. During the test it was noticed that molten aluminium was more inclined to stick (solder) to the H-type samples than to the other specimens, especially at the beginning before the thick oxide layer has developed. The oxide layer protects steel against the molten aluminium as long as it maintains integrity. If it spalls or erodes away, soldering occurs. This is probably why the Al-rich white zones were found only in H- and S-type samples, which have no other protection against molten aluminium besides the oxide layer. The chemical composition of the main zones, revealed in Figures 3 and 4, together with the steel and Al alloy, can be seen in Table 3.

The dark spots seen in Figures 3 and 4 are voids that resulted from the steel manufacturing process. After machining, voids can be exposed on the surface. These sites are more susceptible to thermal fatigue. The situation exacerbates when flaws fill up with oxides, casting alloy or intermetallics, which act as a wedge during the cycling, expanding the cavities. The size of surface defects for the given conditions becomes a

Fig. 3: Pit-like defect of the H4 specimen, 25000 cycles, 2.5% nital, 200×.

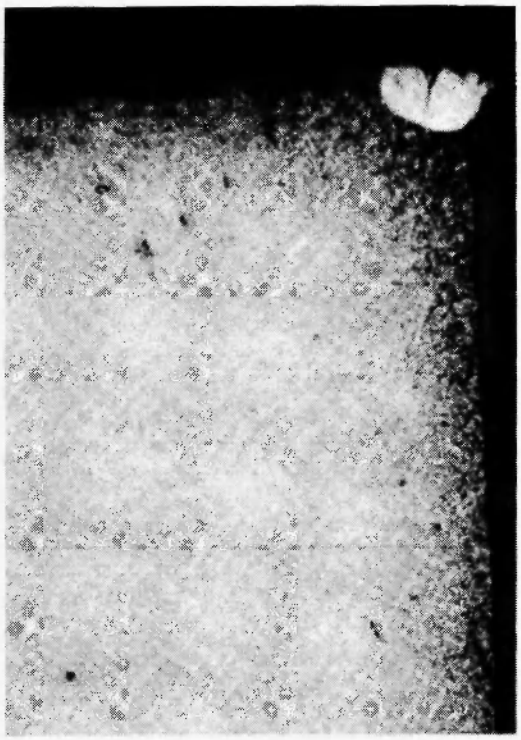

Fig. 4: H4 specimen, 25000 cycles, soldered phase at the corner, 2.5% nital, 200×.

Table 3
Chemical composition (wt %) of the zones in Figures 3 and 4.

Zone	Al	Fe	Si	Cr	V	Mn	S	Hv
Steel	-	91.2	1.0	5.3	1.0	1.5	<0.003	~300
White phase	48.5	42.7	5.6	2.7	0.6	-	-	~1000
Grey layer	-	79.1	3.8	12.2	3.1	-	1.8	~700
LM 24	83	0.8	9.0	0.1	-	0.5	-	-

matter of stress severity, i.e. the bigger the thermal shocks the bigger the surface defects.

S-type Specimens

The transverse crack pattern on the S-type specimens after 25000 cycles is shown in Figure 5. The cracks also have a pronounced tapering shape in the mouth, like those in the H4 specimen, but they are shorter (Table 2).

The changing of the microhardness values of the H and S samples is quite similar (Figure 6), except for the first stage of thermo-cycling (1500 cycles). The S-type specimen shows the better tempering resistance, which can be positively reflected in the delay of crack initiation. Besides that, compressive stresses beneath the

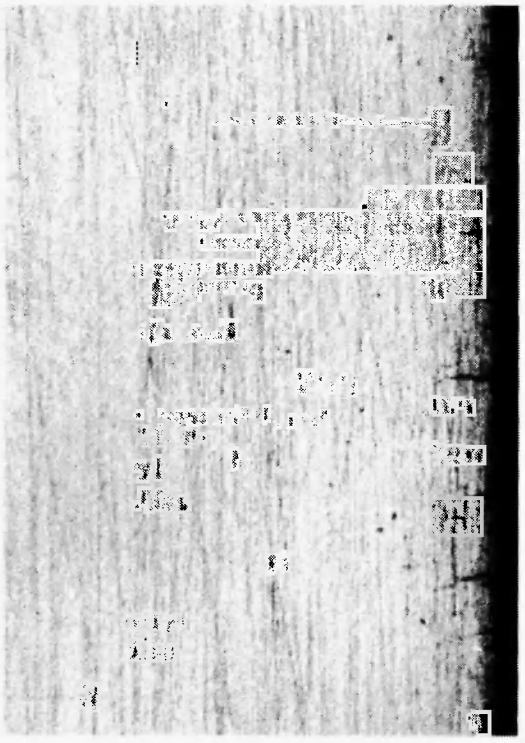

Fig. 5: Transverse crack pattern of the S specimen, 25000 cycles, 25×.

peened surface should have retarded the second thermal fatigue stage – crack propagation.

N-type Specimens

Only N1 sample had a brittle white layer (~5μm) of ε ($Fe_{2-3}N$)- and γ' (Fe_4N)- phases. The depth of the diffusion zone was different for the N1, N2 and N3 specimens – 100, 70 and 40 microns respectively.

Transverse cracks of the all N-type samples are very narrow and hardly visible (Figure 7). This suggests that their openings were retarded by the imposed compressive stresses. Of the specimens already discussed, sample N2 has shown the lowest crack density (Table 2).

The microhardness values of the N2 specimen sit between the values of N1 and N3, which correlates with the length of the nitrogen/carbon diffusion zone (Figure 6). The tempering resistance of the N-type samples is much higher than that of the H-type, which gives the first one more resistance to wear and, in combination with less tendency to soldering, it has more resistance to washout.

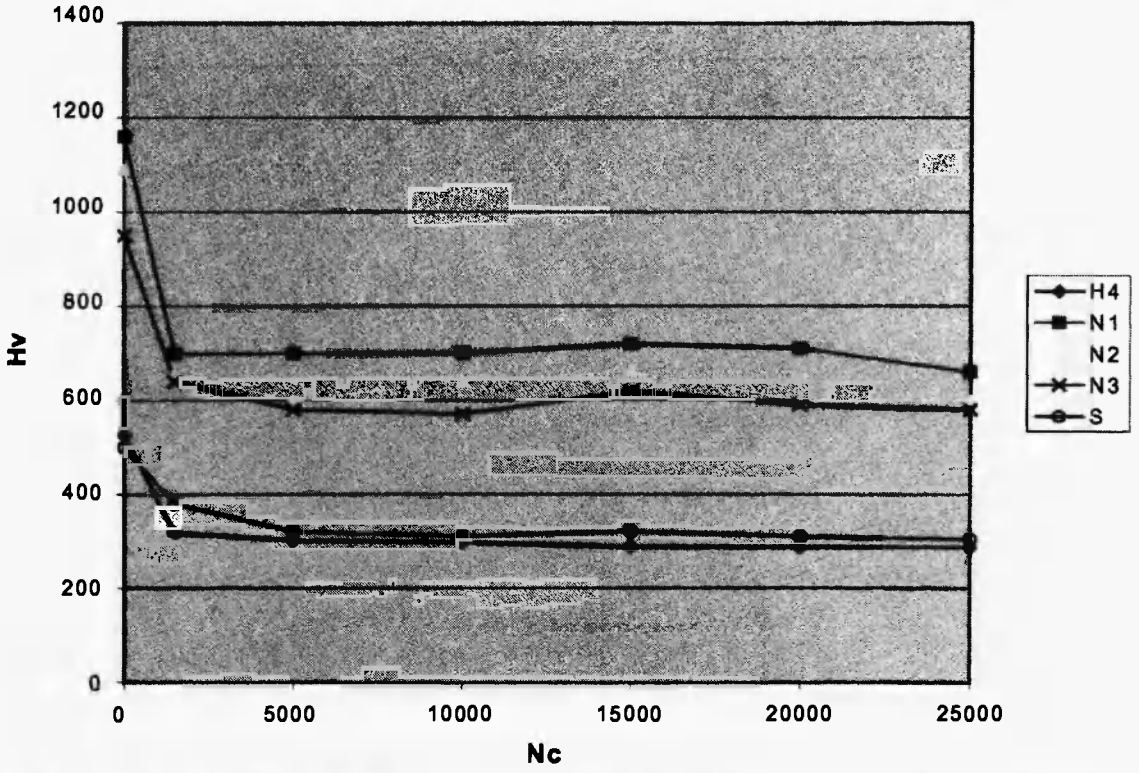

Fig. 6: Case microhardness values (H_V) versus number of cycles (N_C) of the H-, N- and S-type specimens.

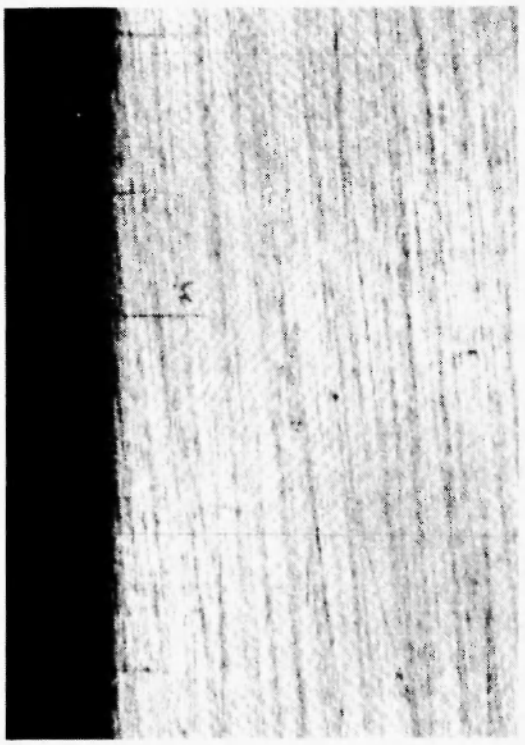

Fig. 7: Transverse crack pattern of the N2 specimen, 25000 cycles, 25×.

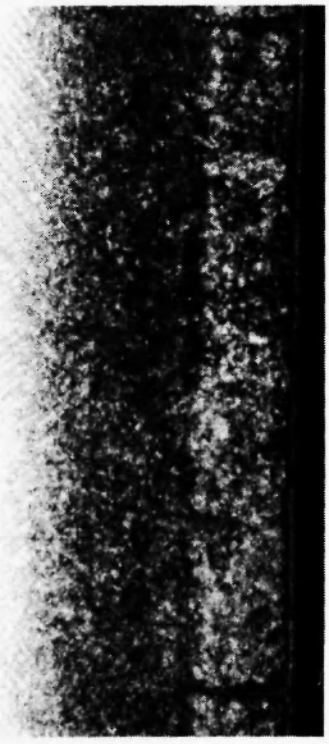

Fig. 8: Longitudinal crack pattern of the N2 specimen, 25000 cycles, 2,5% nital, 200×.

Interesting results were obtained from the cross-sectional examination of the N-type samples (Figure 8). All of them have longitudinal cracks of various depths, but with one common feature – the longest cracks were limited by the depth of the effective diffusion zone (dark strip). Another peculiarity of the longitudinal cracks is that they have already formed after the first 1500 cycles and they have not changed their pattern up to the end of the testing. This means that at the very beginning of the thermo-cycling, cracks initiate quite easily and propagate through the diffusion zone up to the border with the matrix, where they are arrested. Further thermo-cycling is unable to promote the crack growth and initiates only a few more. This phenomenon can be considered as evidence of crack closure and crack arrest features in the diffusion layer due to compressive residual stresses. It can be visualised in terms of a pinched clothes peg model in which the mouth is propped open by a spring, thus introducing compressive stresses in the crack propagation region /8/. The shortest longitudinal cracks were demonstrated by the N3 specimen and this was because it had the smallest effective diffusion depth (~40 μm). The minimal total crack depth and crack density were observed in N2 specimen in spite of the larger effective diffusion depth (~70 μm), which suggests that carbo-nitrides in the surface layer perform better than nitrides for thermo-cycling conditions. Generally, nitride compounds are more brittle than carbo-nitrides and, consequently, they have less ability to accumulate plastic deformation before fracture occurs.

L-type Specimens

The TK6 coating of the L1 sample is metallurgically very well bonded to the substrate, showing no sign of oxidation or other degradation at the interface, with a thickness varying from 3 to 20 μm (Figure 9). Its appearance remains mostly unchanged during the thermo-cycling, but some transformations do occur. Firstly, the coating has lost its continuity in some places (Figure 10). The ESD technique itself is partially responsible for this, because it is quite difficult to maintain the correlation between the electrode

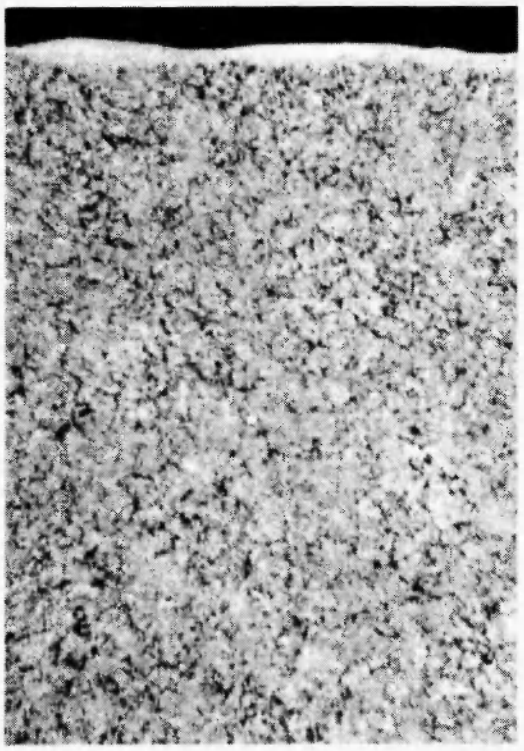

Fig. 9: Initial microstructure of the L1 specimen, 2,5% nital, 200×.

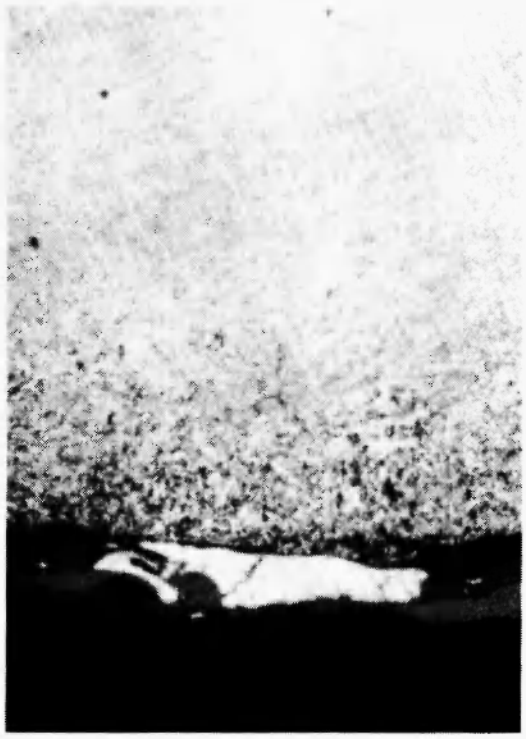

Fig. 10: Microstructure of the L1 specimen, 25000 cycles, 2,5% nital, 500×.

displacement and its geometry. This problem can be overcome by doing a second pass. Secondly, partial decomposition of the tungsten carbide can also be responsible for that. The chemical composition of the main zones and layers revealed in Figure 10 (innermost dark layer, inner layer, outer layer and white TK6 coating) is presented in Table 4. The XRD peaks have shown the presence of tungsten carbide, complex oxides of Fe, Cr, Co and V enriched, probably, by Si and S. All these elements are included in the steel composition, and sulphur has come from the anti-soldering paste, which contains sulphuric acid. The formation of all these phases is as a result of reaction between the steel, coating, anti-soldering paste, lubricant and aluminium melt, involving a simultaneous diffusion and dissolution at the corresponding interfaces. Neither W nor Co was detected either in the outer oxide layer or in the substrate. The reason for this is, probably, because they were in trace amounts below detection limits. Therefore, if the partial decomposition of tungsten carbide does occur, the inward carbon diffusion to the substrate can take place. The substrate hardness values of the L1 and L3 specimens increase after 10000 cycles (Figure 11), which supports the above assumption.

The initial microstructure of the L2 specimen has a remelted surface of 30 – 50 μm in depth, where all precipitated carbides are dissolved in the matrix (Figure 12). During the first thermo-cycling stage (1500 cycles), the carbide precipitation is restored and the microstructure remains unchanged up to the end of the test.

The initial microstructure of the L3 specimen (Figure 13) appears as a combined pattern of the L2 remelted zone and the well metallurgically bonded TK6 coating of the L1 sample. On the other hand, some very small discontinuities (cracks, dot-like porosity) can be detected in the ESD coating of the L3 specimen (Figure 13). During the test, the microstructure transformation of the L3 coating followed a similar pattern as the L1 sample (Figure 10).

The L3 specimen exhibited the lowest crack parameters of all tested samples (Figure 14 and Table 2).

Table 4
Chemical composition (wt %) of layers in Figure 10.

Layer	Fe	Si	Cr	V	Mn	W	Co	S
Steel	91.2	1.0	5.3	1.0	1.5	-	-	<0.003
Innermost dark layer	76.0	4.5	13.1	4.9	-	-	-	1.5
Inner grey layer	92.8	-	5.4	1.5	-	-	-	0.3
Outermost dark layer	78.8	3.5	12.7	3.1	-	-	-	1.9
White coating	27.4	-	0.9	-	-	65.5	6.5	0.8

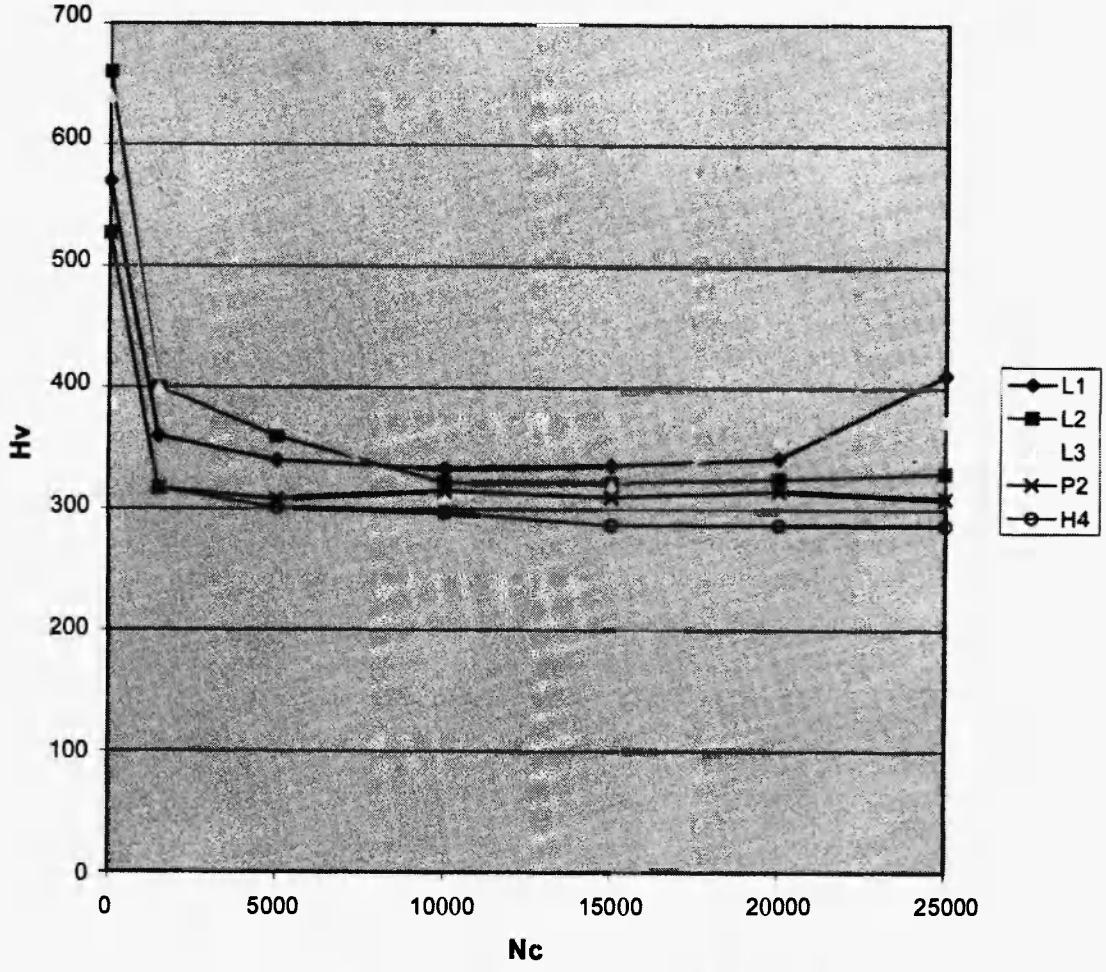

Fig. 11: Substrate microhardness values (H_V) versus number of cycles (N_C) of the H-, L1-, L2-, L3- and P2 specimens.

Fig. 12: Initial microstructure of the L2 specimen, 2,5% nital, 500×.

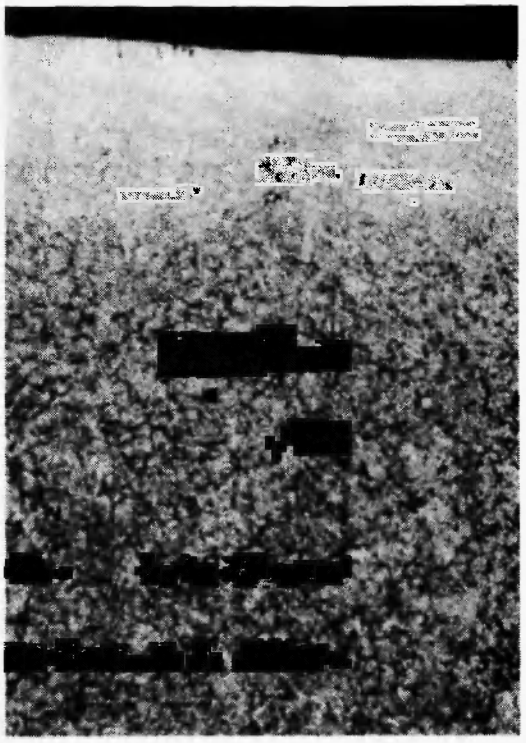

Fig. 13: Initial microstructure of the L3 specimen, 2,5% nital, 200×.

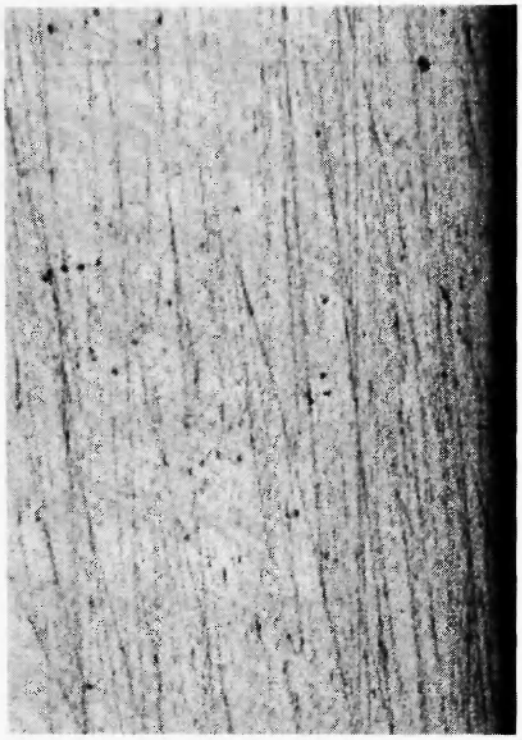

Fig. 14: Transverse crack pattern of the L3 specimen, 25000 cycles, 25×.

P-type specimens

The initial microstructure of the plasma-sprayed specimen P2 with the cobalt-based superalloy coating features some porosity (Figure 15). During the thermo-cycling, oxidation at the coating/substrate interface has occurred. At macrostructural level, the coating has cracked and spalled at some places at the corners. In spite of all this, the sample has withstood the whole testing program and the substrate under the coating has shown less cracking than the uncoated H4 specimen (Figure 16). The mechanism of crack retarding of the P-type specimen is different from the L-type one, because of the different substrate/coating bonding. The main reason for the P-type crack pattern improvement is, probably, due to the thermal gradient decreasing.

The changes in the coating microhardness values of the coated samples as a function of the number of cycles are shown in Figure 17 (uncoated H4 and L2 are presented for comparison). The substantial increase of the hardness for the P2 coating during the first 1500 cycles can be explained as a result of phase

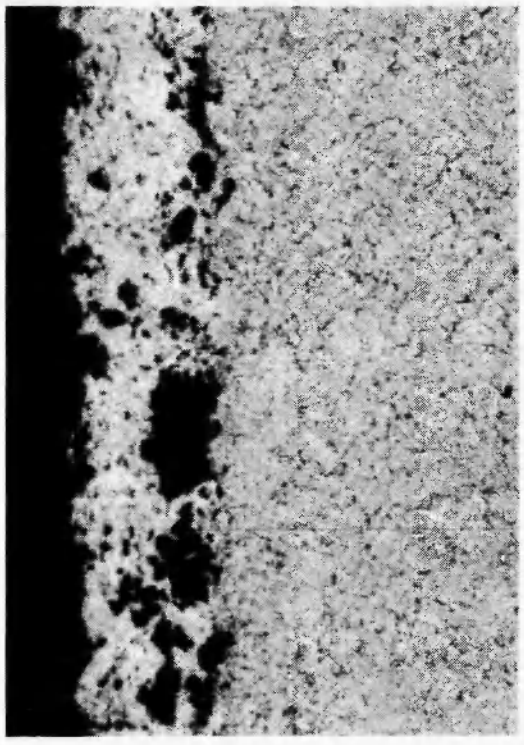

Fig. 15: Initial microstructure of the P2 specimen, 2,5% nital, 200×.

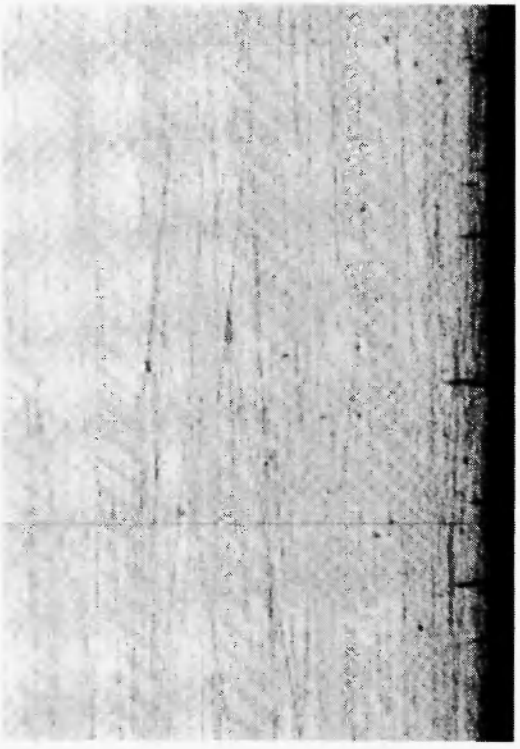

Fig. 16: Transverse crack pattern of the P2 specimen, 25000 cycles, 25×.

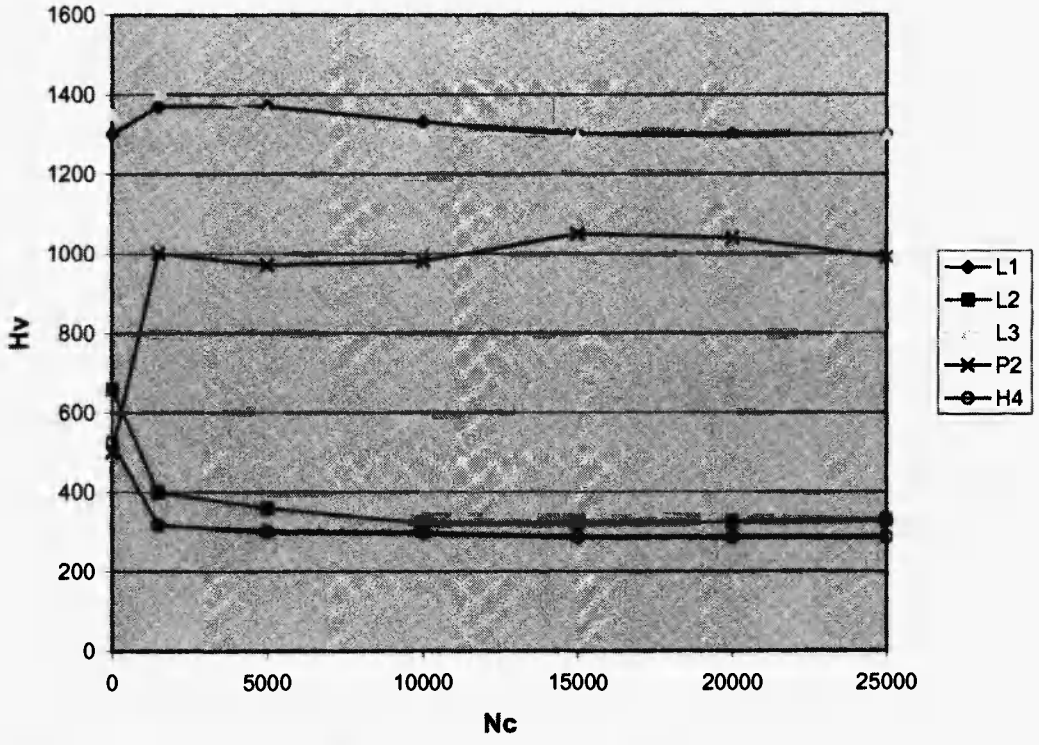

Fig. 17: Case microhardness values (H_V) versus number of cycles (N_C) of the H-, L1-, L2-, L3- and P2 specimens.

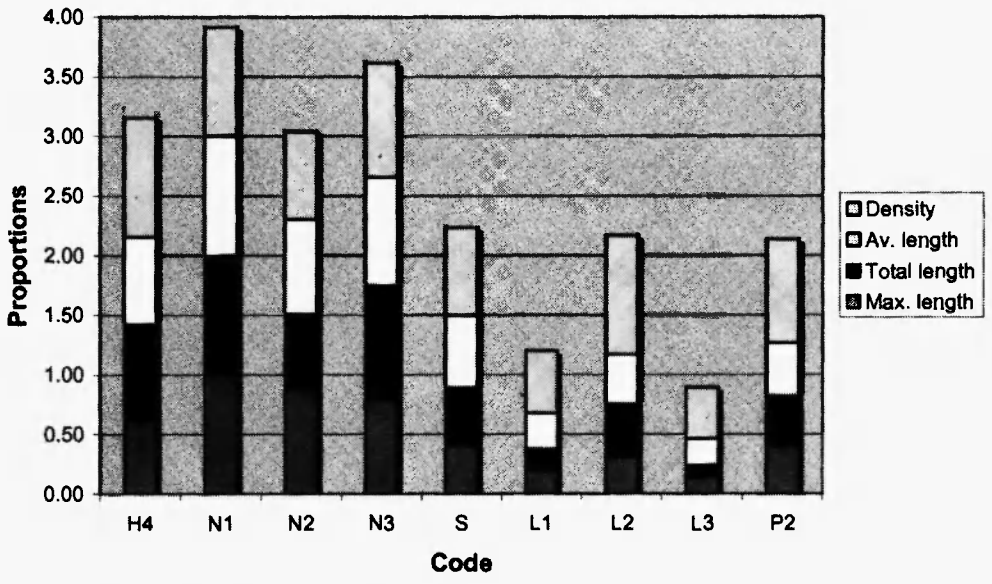

Fig. 18: Cumulative relative crack parameters of the tested specimens.

transformations, which include the secondary hardening (precipitation of various secondary carbides or the like).

The accumulated index of all crack parameters (l_{max}, Σl_{max}, l_{av} and n), where the worst one in each group was taken for unity, and the others expressed as a fraction of that, is shown in Figure 18. The L-, P-, and S-type specimens have demonstrated an improved thermal fatigue resistance compared to the bare H4 and nitrided N-type samples. For all parameters, the L3 specimen has performed the best, which is likely to involve both delaying crack nucleation and growth due to the coating's high hot hardness, low thermal expansion and high residual compressive stresses.

CONCLUSIONS

1. The H-type samples were the only specimens which have shown "pit-like" defects. This is because they had the lowest surface hardness and, as a consequence, inferior heat checking and erosion resistance.
2. The soldered intermetallic phases were found only in the H- and S-type specimens. The oxide layer protects steel against the molten aluminium as long as it maintains integrity. If it erodes away for any reason, soldering and wash out occur.
3. The N-type samples were the only ones in which longitudinal cracks were found and, moreover, they appeared during the first 1500 thermo-cycles. The maximum crack depth and average crack depth have shown a strong dependence on the effective diffusion zone depth, at the border of which cracks become arrested and do not propagate further during subsequent thermo-cycling. The N2 specimen had the smallest total crack depth and density independently of the diffusion depth, which means that a carbo-nitrided surface resists crack initiation better than a nitrided one.
4. The transverse cracks of the N-type specimens are very narrow and hardly visible. This suggests that their opening was retarded by the imposed compressive stresses. The combined average indices of the longitudinal crack parameters are similar for the H4 and N2 samples.
5. The tempering resistance of the N-type specimens is much higher than that of the H-type one, which makes them more resistant to wear and, in combination with less soldering tendency, more resistant to washout.
6. The S-type specimen has shown the shortest crack lengths compared to the H4 and N-type specimens, with more pronounced tapering structure in the

mouth. This may imply that the cracks were opening up.

7. The substrate of the plasma-sprayed specimen P2 has shown an improved thermal fatigue resistance, but the coating itself has cracked and spalled off the corners. Assuming that there was an inadequate substrate/coating bonding, a reasonable explanation for the retarding of steel cracks may be because of a reduced thermal gradient due to the coating.
8. The ESD L-type specimens have shown the lowest thermal crack pattern, which is likely to involve both delaying crack nucleation and growth due to the coating's high hot hardness, low thermal expansion and high residual compressive stresses.
9. The TK6 coating has an excellent metallurgical bond to the substrate, but at some places it has lost the continuity due to insufficient electrode overlapping and, probably, to the partial decomposition of the tungsten carbide.
10. The high and stable tempering resistance of the hard coatings, which reduces wear, combined with less affinity to the molten aluminium and thermal fatigue inhibiting, may contribute to a substantial die life increase.
11. The thermal fatigue resistance of the bare H4 sample had an improvement of 20% by using the shot peening, 33% by using the laser hardening and plasma spraying, 260% by using the electro spark deposition of TK6 and 400% by using the laser hardening/TK6 coating.

ACKNOWLEDGEMENTS

This project was supported by the Technology New Zealand, The University of Auckland and Glucina Smelters Limited, New Zealand.

REFERENCES

1. L. Liimatainen and A. Ranta-Eskila, *Die Cast. Eng.*, 1991.
2. S.S. Manson, *Thermal Stress and Low-Cycle Fatigue,* McGraw Hill, New York, 1966.
3. D. Delagness, C. Levaillant, F. Rezai-Aria, and A. Grellier, *20th Die Casting Congress and Exposition,* November 1-4, 1999, Cleveland, Ohio, T99-105.
4. S. Malm and L-A. Norstrom, *Met. Sci.*, **1979,** 544.
5. S. Gopal, A. Lakare, and R. Shivpuri, *Surf. Engineering,* **15,** 4 (1999).
6. S. Wang, Y. Li, M. Yao and R. Wang, *Journa. of Mater. Proces. Technol.*, **1998,** 73.
7. D.T. Fraser, M. Jahedi and Z.W. Chen, *Die Casting & Toolmaking Technology Conf.,* 22-25 June 1997, Melbourne, 97/25.
8. B.L. Averbach, B. Lou, P.K. Pearson, *et al, Metallur. Transac.*, **16**A, July (1985).